Flexible Optical Cross-Connects for High Bit Rate Elastic Photonic Transport Networks [Invited]

M. Song, E. Pincemin, A. Josten, B. Baeuerle, D. Hillerkuss, J. Leuthold, R. Rudnick, D. M. Marom, S. Ben Ezra, J. F. Ferran, G. Thouenon, P. S. Khodashenas, J. M. Rivas-Moscoso, C. Betoule, D. Klonidis, and I. Tomkos

***Abstract*—We present here the work performed in the EU-funded flexible optical cross-connect (FOX-C) project, which investigates and develops new flexible optical switching solutions with ultra-fine spectral granularity. Thanks to high spectral resolution filtering elements, the sub-channel content can be dropped from or added to a super-channel, offering high flexibility to optical transport networks through the fine adaptability of the network resources to the traffic demands. For the first time, the FOX-C solutions developed in the project are investigated here and evaluated experimentally. Their efficiency is demonstrated over two high spectral efficiency modulation schemes, namely multi-band orthogonal frequency division multiplexing (MB-OFDM) and Nyquist WDM (N-WDM) formats. Finally, in order to demonstrate the relevance of the FOX-C node concepts, a networking study comparing the economic advantages of the FOX-C optical aggregation solution versus the electronic one is performed.**

***Index Terms*—Elastic optical networking; Flexible optical cross-connect; MB-OFDM; N-WDM; Optical versus electronic aggregation.**

I. Introduction

In the post-wavelength division multiplexing (WDM) era, the intensive research on innovative data transport technologies and network architectures has identified the elastic optical networking concept [1] as one of the key enablers for increasing traffic while delaying the expected "capacity crunch." Additionally, a shift of the traffic profile toward rich content video and cloud services is nowadays obvious, imposing high peak-to-average traffic ratios, which result in large bandwidth and capacity variations over time. The key characteristic of elastic (also referred to as flexible) optical networking (EON) [2] is that the network resources are continuously adapted to the traffic demands. Thus, optimized resource utilization is maintained, avoiding the need for over-provisioning due to high traffic fluctuations.

In EON, the adaptability of the network resources to the traffic demands is determined by the characteristics of the defined super-channel (Sp-Ch) and corresponding switching capabilities. A Sp-Ch is formed as one contiguous spectral entity with variable bandwidth that is adapted to the capacity of each demand (or aggregation of demands with the same networking requirements). The key characteristic of a Sp-Ch is that it is composed of multiple carriers that are usually set very close to one another with minimal guard-bands between carriers with the goal to achieve both high spectral efficiency and high capacity channels [1,3]. Modulation schemes that are compatible with such requirements are, for instance, the spectrally overlapped orthogonal frequency division multiplexing (OFDM) format in its multi-band approach (MB-OFDM) and the time-overlapped Nyquist-wavelength division multiplexing (N-WDM) format, each one being implemented either in the optical or electronic domain [2]. On the other hand, the properties of the bandwidth adaptive switch determine the EON capabilities and the routing of the Sp-Ch entities [4,5]. Wavelength selective switches (WSSs) are the key network elements of EON with flexible bandwidth characteristics that can be dynamically adapted to the Sp-Ch bandwidth as the Sp-Ch is routed through the network.

Although the commonly defined Sp-Ch entity in EON addresses the capacity-on-demand issue, it relies on electronic aggregation functions at each node. Thus, switching can only be performed transparently at the Sp-Ch level in a similar way to WDM but with the use of flexible bandwidth WSSs. Any processing of the Sp-Ch contents (typically with ultra-dense spectral allocation) requires first the reception of the whole Sp-Ch in the node and the electronic processing and switching of its contents. Also, even when switching at the Sp-Ch level is assumed, spectral gaps are required to be inserted between the neighboring Sp-Chs in order to prevent crosstalk. In this case, the switching granularity is restricted to that of the Sp-Ch level, and although in general the minimum Sp-Ch bandwidth can

Manuscript received February 1, 2016; revised April 20, 2016; accepted May 6, 2016; published June 13, 2016 (Doc. ID 258706).

M. Song, E. Pincemin (e-mail: erwan.pincemin@orange.com), G. Thouenon, and C. Betoule are with Orange Labs, 22300 Lannion, France.

A. Josten, B. Baeuerle, D. Hillerkuss, and J. Leuthold are with ETH Zurich, 8092 Zurich, Switzerland.

R. Rudnick and D. M. Marom are with the Hebrew University of Jerusalem, 91904 Jerusalem, Israel.

S. Ben Ezra is with Finisar Ltd Israel, 74140 Nes-Ziona, Israel.

J. F. Ferran is with W-Onesys, 0872 Barcelona, Spain.

P. S. Khodashenas, J. M. Rivas-Moscoso, D. Klonidis, and I. Tomkos are with Athens Information Technology, 15125 Marousi, Greece.

http://dx.doi.org/10.1364/JOCN.8.00A126

be flexibly defined, the required insertion of a spectral gap between Sp-Chs reduces notably the overall spectral efficiency.

The work performed here investigates and develops novel elastic switching solutions [6,7] and the related enabling technologies [8] to offer dynamic aggregation and switching at the Sp-Ch contents level, defined as the sub-channel (Sb-Ch) level. Such all-optical traffic grooming solutions can achieve ultra-small switching granularity, resulting in significantly enhanced spectral utilization and reduced energy consumption compared to electronic traffic aggregation schemes. Moreover, the enhanced granularity offered by all-optical switching solutions enables the redefinition of the Sp-Ch entity in EON in terms of traffic allocation flexibility and the increase of spectral utilization, leading correspondingly to the increase of network spectral efficiency.

In this paper, the overall flexible optical cross-connect (FOX-C) node design concepts are first presented in Section II, followed by an overview of the enabling switching technologies in Section III. The experimental performance evaluation of the proposed node is described and presented in Section IV. Finally, Section V includes the related network evaluation studies and the expected benefits from the adopted concept.

II. FOX-C Node Concepts

The main goal of the FOX-C node is to provide optical switching of low rate tributaries (i.e., Sb-Ch) directly from multiple ultra-high capacity Sp-Ch links. It is noted that typically in literature the term Sp-Ch has been used to describe a signal that consists of multiple carriers that may originate from the same laser source [9] or individual lasers [10], yet it is perceived as a single entity. Regardless of the technology used to generate it, the Sp-Ch is an ultra-high bit-rate channel that is transmitted and received (in whole or in part [11,12]) as a continuous waveband signal formed by combining several low data-rate sub-carriers. In that sense, a Sp-Ch does not necessarily have the ability to add/drop some of its sub-carriers at an intermediate node along its route.

Here, the Sp-Ch approach considers a dynamically adaptable waveband that is assigned coarsely on an end-to-end basis (according to slowly varying traffic demands between nodes), while it is able to add/drop or even switch some of its contents. Thus, the term “sub-channel” or “sub-band” is introduced to define the data that are carried by an optical carrier within a Sp-Ch. In this context, a variable number of Sb-Chs form the Sp-Ch content.

Therefore, the new flexible optical networking scheme, promoted by the technologies at the core of the FOX-C node concept, defines three levels of data grooming, as depicted in Fig. 1. According to this, low rate tributary connections are combined to form sub-channels (at level 1), which in turn are multiplexed to form spectrally efficient and ultra-high capacity super-channels (at level 2) and finally multi-terabit optical link connections (at level 3).

In turn, the signal transitions (from one multiplexing level to another one) define two switching granularity levels per fiber. As a result, the designed FOX-C switching node architecture is based on two switching levels that address a coarse switching resolution level (when Sp-Chs are extracted from or added to the WDM link) and a fine

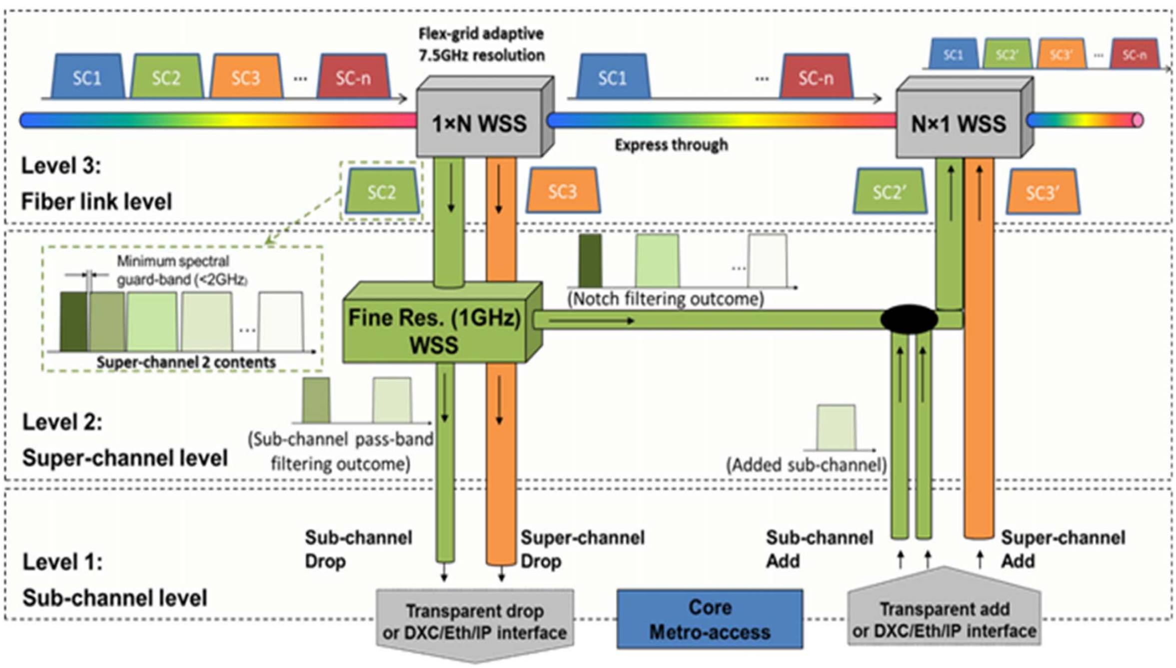

Fig. 1. Functional elements of a flexible optical node with ultra-fine switching granularity following the three hierarchy levels defined by the FOX-C project (SC: super-channel).

switching resolution level (when the contents of the Sp-Ch—i.e., the Sb-Chs—are processed).

The design and key enabling technologies for the realization of this multi-level node design with transparent switching capabilities at the Sb-Ch level are presented in the next section.

III. Filtering and Switching Elements of the FOX-C Node

The operating principle of a high spectral resolution (HSR) optical filter [7], used as a building block for the fine resolution WSS shown in Fig. 1, is similar to that of a WSS with a liquid crystal on silicon (LCoS) processor for flexible bandwidth allocation [see Fig. 2(a)]. However, the bulk diffraction grating dispersive element is replaced by an engineered phase array waveguide grating (AWG) designed to provide fine optical resolution over a finite bandwidth. A state-of-the-art phase array implemented in a silica-on-silicon platform was reported in [6], where a high resolution AWG was designed to achieve <1 GHz optical resolution (i.e., the edge roll-off bandwidth from −0.5 dB or 90% down to −10 dB or 10%) and 400 MHz spectral granularity (i.e., the tuning precision for the filter edge placement) while operating over a 200 GHz free spectral range (FSR). Since the length difference between the shortest and longest waveguides is ~250 mm in silica waveguides (to obtain the <1 GHz resolution), the waveguides are folded three times within the planar lightwave circuit (PLC), as shown in Fig. 2(b), resulting in a total size of 50 mm × 10 mm.

The multi-port HSR filter, depicted in Fig. 2(a), can consist of a stack of AWGs, each representing an input/output port, a free-space optical arrangement for dispersing the optical signal onto an LCoS spatial light modulator (SLM), itself controlled by a computer that can assign spectral quanta as fine as the spectral granularity to subdivide the Sp-Ch into its finer tributaries. The corresponding insertion losses are typically ~15 dB. With a higher integration level in the next version of the filter, the level of losses should be significantly reduced. One fiber port (i.e., one of the AWGs) accepts a Sp-Ch of any bandwidth up to the FSR limit of the AWG. The Sp-Ch is then dispersed with a lens on the LCoS-SLM at fine resolution. The LCoS-SLM selects the spectral bandwidth (which can be adapted to the spectral width of one or several Sb-Chs) that will be routed to an individual output AWG. This output AWG is assigned to a "drop" side (where the filter performs a pass-band function) and a "through" destination (where the filter realizes a stop-band function), which will then be re-multiplexed with new "add" data to form the new Sp-Ch for upstream transmission, as depicted in Fig. 1. Since the optical resolution of the AWG is at record fidelity, the band transitions are extremely sharp, enabling the separation of the Sp-Ch into any combination (not necessarily spectrally contiguous) of its tributaries with minimal guard-bands.

In Fig. 2(c), the calculated finer HSR filter performance characteristics are shown where variable bandwidth channels are deployed at a spectral granularity of 400 MHz (denoted by vertical grid lines) and an optical resolution of 1 GHz. This reveals the capability to extract even 10 GHz channels with a minimum spectral guard-band of 2 GHz between them while achieving crosstalk suppression close to 25 dB. The versatility of the AWG-based HSR filter is enabled by LCoS-SLM processing, which is applied to the spatially dispersed light independently of the dispersion scheme. However, the challenge of this approach is the accuracy to which the AWG must conform. Briefly stated, all the AWG's arms must radiate at the exact same relative phase while providing path length differences required to provide the spectral resolution value. Two techniques for correcting fabrication phase errors have been successfully demonstrated by the results obtained in [6,13].

IV. FOX-C Node Performance Evaluation

In this section, we report the preliminary results of the FOX-C node system evaluation. First, the FOX-C node, which integrates the previously described HSR filter, is introduced between a MB-OFDM or N-WDM transmitter and a coherent receiver for back-to-back characterization. Second, it is inserted in the middle of an N × 100 km G.652

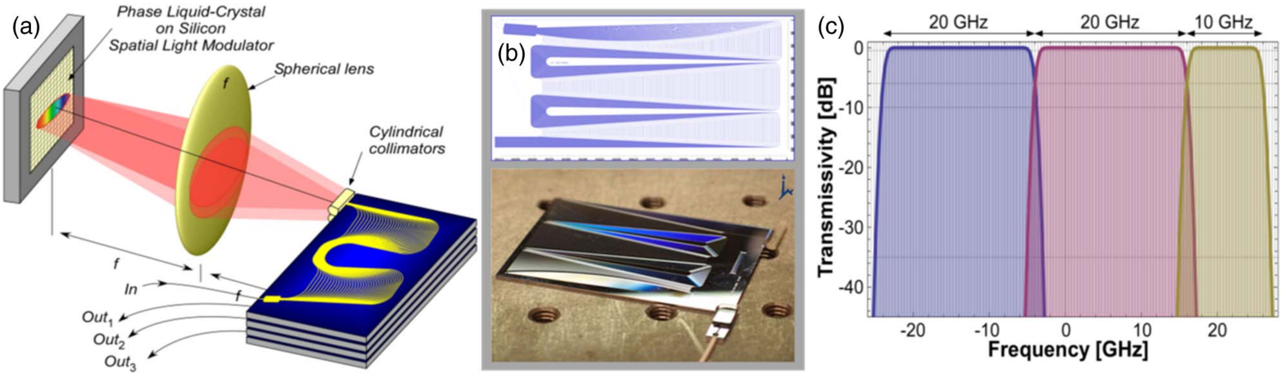

Fig. 2. (a) Fine-resolution WSS based on a high resolution filter employing one input and several output AWGs for high resolution dispersion as well as an LCoS switching engine; (b) AWG design and implementation providing <1 GHz optical resolution and 400 MHz spectral granularity; (c) calculated fine spectral filter performance characteristics for three flexible Sb-Chs.

fiber line for transmission evaluation. To be efficient, the HSR optical pass-band and stop-band filters have to be ultra-selective to extract and/or suppress very narrow sub-channels (also referred to as sub-bands). A rectangular transfer function is required to minimize the distortions undergone by the Sb-Chs during the add/drop process.

A. MB-OFDM and N-WDM System Descriptions

Two modulation format types have been chosen and compared. Due to their high flexibility and rectangular spectrum, MB-OFDM and N-WDM formats are interesting candidates for upcoming elastic optical transport networks (OTNs) operating at the Sb-Ch level.

One terabit per second coherent dual-polarization MB-OFDM and N-WDM Sp-Chs are used for the evaluation. They are composed of 10 Sb-Chs with 20 GHz spacing, each carrying a 100 Gbps net data rate that constitutes the 1 Tbps Sp-Ch. After including the 20% forward error correction (FEC) overhead and the 20% OFDM overhead for data-aided equalization, the gross bit rate of each OFDM sub-band becomes 144 Gbps, resulting in bandwidth of 18 GHz and guard-band of 2 GHz between the Sb-Chs. Blind equalization is performed for N-WDM Sb-Chs, and as a result only 20% FEC overhead is required, resulting in Sb-Chs of 120 Gbps raw bit rate, bandwidth of 15 GHz, and guard-band of 5 GHz. The total bandwidth of the Sp-Ch is thus ~200 GHz, which corresponds to a net spectral efficiency of ~5 bits/s/Hz. Spectra of the generated Sp-Chs are depicted in Fig. 3. Each Sb-Ch inside the Sp-Ch has a flat spectrum because amplitude pre-emphasis is performed at the transmitter side.

At the transmitter side (shown in Fig. 4), the hardware used for the generation and detection of MB-OFDM and N-WDM Sp-Chs is identical. Two digital-to-analog converters (DACs) embedded into a 15 GHz bandwidth Keysight 8195A AWG operating at 64 GSamples/s produce the in-phase (I) and quadrature (Q) components of the complex signal. The OFDM symbols are generated and detected using 1024-point fast Fourier transform/inverse fast Fourier transform (FFT/IFFT) operations among which 576 sub-carriers are loaded with a 16QAM (quadrature amplitude modulation) symbol constellation. A sequence of 32 training symbols [0 TS 0 TS … 0] is inserted at the frame's beginning for synchronization, carrier frequency offset (CFO) estimation, and channel equalization (including polarization separation). Sixteen pilot tones are dedicated to phase noise compensation. A cyclic prefix of 128 samples (4.5 ns) is added at the beginning of each OFDM symbol to provide robustness against inter-symbol interference (ISI) and more particularly against chromatic dispersion (17,000 ps/nm of cumulated dispersion is considered here). The 20% overhead required for FEC, plus 12.5% for cyclic prefix, 3.6% for training symbols, and 2.8% for pilot tones, leads to a global data rate of 144 Gbps for one OFDM Sb-Ch signal. After amplification by two linear RF drivers, the I and Q tributaries feed a complex Mach–Zehnder modulator (CMZM). Polarization multiplexing is then performed by introducing a one-symbol delay (~36 ns) between the two

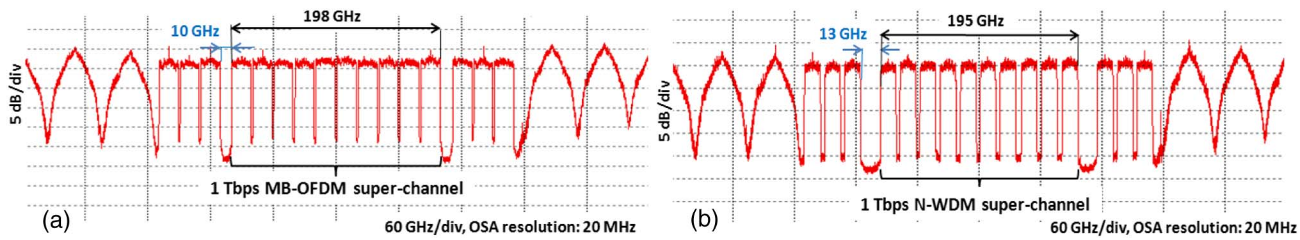

Fig. 3. Spectra measured with a high-resolution optical spectral analyzer (20 MHz) of the 1 Tbps Sp-Ch and WDM multiplex used in the experiments: (a) MB-OFDM, (b) N-WDM.

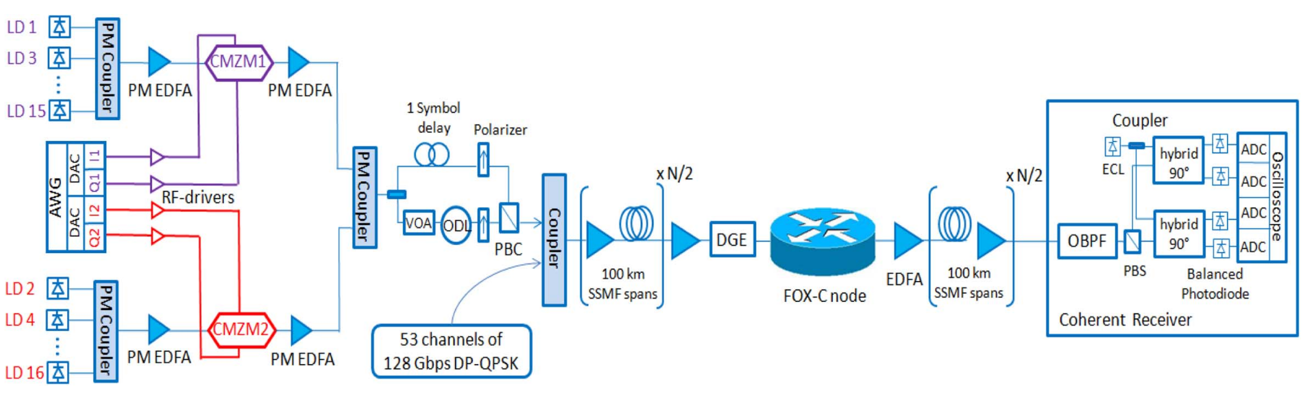

Fig. 4. Experimental setup showing the MB-OFDM or N-WDM transmitter, N × 100 km G.652 fiber-based transmission line, and coherent receiver (N = 4, 6, 8, 10).

replicas of the OFDM signal, which are subsequently coupled by the means of a polarization beam combiner (PBC). The main steps of digital signal processing (DSP) implemented at the receiver side [12,14] are symbol synchronization [15], fractional and integer CFO compensation [16], cyclic prefix removal, frequency domain conversion using FFT, channel estimation and zero-forcing equalization for gain/phase distortion compensation and polarization separation [17], and finally laser phase noise compensation through the pilot tones method [18].

The 100 Gbps dual-polarization N-WDM Sb-Chs support a 20% overhead corresponding to the FEC insertion, leading to a gross data rate of 120 Gbps. The pulse shaping is performed using a root-raised-cosine filter with a roll-off factor of 0.05. The information bits are mapped on complex 16QAM symbols at a symbol rate of 15 Gbaud. Differential encoding is carried out to overcome phase ambiguities. The same linear RF drivers and CMZM employed for OFDM are then used to encode the data on the optical carrier. The polarization multiplexing device is identical to that previously described, except for the time delay (~36 ns), which is adjusted to be a strict multiple of the symbol duration. The transmitter DSP implemented at the N-WDM transmitter side can be decomposed as follows. After differential encoding and Nyquist filtering, pre-equalization is applied over the signal in order to compensate for the amplitude and phase distortions of the transmitter. The pre-distortion is implemented by a frequency domain equalizer using the "overlap and save" method.

At the receiver (Rx) side, DSP is based on blind equalization in order to avoid any additional overhead and therefore maximize the spectral efficiency. After static frequency domain compensation of chromatic dispersion, the recorded waveform is normalized and de-skewed in order to compensate for the transceiver imperfections (IQ imbalance or various path lengths). The received waveform is matched-filtered with a root-raised-cosine filter, which is the counterpart of the pulse shaping filter used at the transmitter side. The sampling offset is compensated by a special timing recovery technique based on the modified Godard algorithm and afterward re-sampled to two samples per symbol [19]. The two polarizations are demultiplexed, and the signal is compensated for polarization mode dispersion (PMD) and residual chromatic dispersion. This is done in a 2×2 butterfly finite impulse response (FIR) filter structure with 9 taps, which can dynamically mitigate the channel impairments. After a pre-convergence step based on the constant modulus algorithm (CMA) [20], the equalizer is switched to the radius-directed equalization (RDE) method [21]. The carrier frequency offset compensation is performed by observing the peak of the spectrum of the mth power signal [22]. The carrier phase compensation comprises two stages; the first stage uses the blind phase search method [23], while the second stage implements the maximum likelihood phase estimation technique [24]. After carrier recovery, a third equalization stage is applied to further improve the signal quality and eliminate linear signal distortions. This step is realized thanks to a T-spaced decision-directed least mean square (DD-LMS) equalizer with 61 taps. Finally, demodulation is achieved considering differential decoding.

Figure 4 shows the transmitter (Tx) and receiver setup. The 1 Tbps MB-OFDM or N-WDM Sp-Ch is generated thanks to ten 100 kHz linewidth external cavity lasers (ECLs) spaced by 20 GHz, which feed two CMZMs. By means of two independent pairs of DACs, data carried by the neighboring sub-bands are totally de-correlated, provided that the first pair of DACs generates the odd Sb-Chs, while the second pair generates the even Sb-Chs. Six complementary distributed feedback lasers (DFBs) are used to produce six other OFDM or N-WDM Sb-Chs (three on each side of the 1 Tbps Sp-Ch), which are introduced to emulate fiber nonlinearities. They are located at 10 GHz from the last right/left-hand Sb-Ch of the Sp-Ch in the case of OFDM and at 13 GHz in the case of N-WDM. The 16 Sb-Chs are combined together by means of two stages of 8:1 and 2:1 polarization-maintaining (PM) couplers. Two PM erbium-doped fiber amplifiers (PM-EDFA) are inserted to balance the coupler losses. Finally, the 16 sub-bands are combined with 53 channels, each carrying 128 Gbps dual-polarization quaternary phase shift keying (DP-QPSK) modulation, which fill the EDFA bandwidth and emulate fiber nonlinearities.

At the receiver side, the sub-band under measurement and its immediate neighbors are selected by a square flat-top optical pass-band filter (OPBF) of 0.5 nm bandwidth and detected by a polarization diversity coherent receiver using a 100 kHz linewidth ECL as local oscillator (LO). The signals are converted back to the digital domain thanks to four analog-to-digital converters (ADCs) operating at 50 GSamples/s embedded into a Tektronix DPO 72004C real-time storage oscilloscope. The LO wavelength is tuned to the center of the Sb-Ch under measurement. The received waveforms are stored in the scope memories and sent to a computer in which the DSP previously described is performed.

B. FOX-C Node Performance in Back-to-Back

The main objective of the back-to-back (BtB) characterization is to determine the optimal bandwidth of the optical pass-band and stop-band filters, which are inserted into the FOX-C node. Thus, the introduction of the HSR optical add/drop multiplexing (OADM) function does not induce much performance penalty through filtering imperfections and/or signal crosstalk.

The FOX-C node is built for the tests as follows (see Fig. 5). At its input, a flexgrid LCoS-based WSS (typical switching time <500 ms) extracts the 1 Tbps Sp-Ch and sends it over one of its outputs. On a second output, the LCoS-WSS sends the remaining WDM multiplex, from which the Sp-Ch has been removed. The Sp-Ch present over the lower output arm of the WSS is replicated by means of a 1:2 coupler. The first signal replica is used for the "drop" operation. The HSR-OPBF extracts the sixth sub-band from the Sp-Ch. The second copy on the upper arm of the 1:2 coupler is sent into a HSR optical stop-band filter (HSR-OSBF), which deletes this sixth Sb-Ch from the

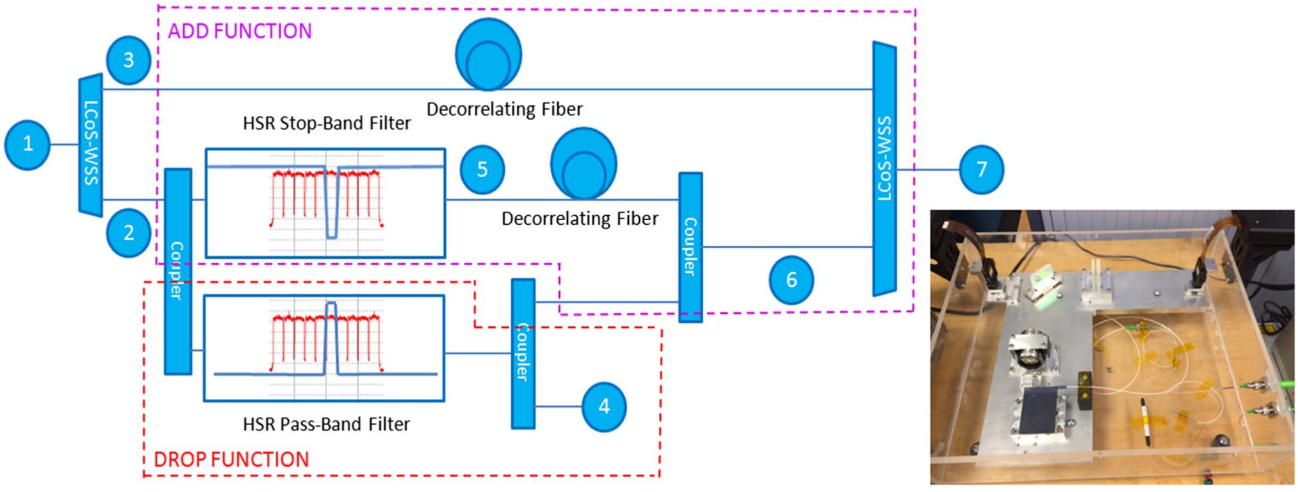

Fig. 5. Setup of the FOX-C node with its two levels of optical switching at the Sp-Ch and Sb-Ch levels. Branch 3 is labeled "remaining WDM multiplex." Branch 2 corresponds to the "Sp-Ch Drop," and branch 6 to the "Sp-Ch Add." Branch 5 corresponds to the "remaining Sp-Ch through," while the two outputs of the internal 1:2 coupler are "Sb-Ch Drop" (labeled 4) and "Sb-Ch Add" (top). Inset: HSR optical filter capable of operating as pass-band and stop-band filters. In the experiments shown, it is used as a pass-band filter.

Sp-Ch. Note that this commercial HSR-OSBF has a better extinction ratio (~40 dB) than the HSR-OPBF. A second 1:2 coupler is added in order to duplicate the extracted sixth sub-band. The copy present on the lower arm of the coupler is used for measurements and optimization of the HSR-OPBF bandwidth. The sixth Sb-Ch replica on the upper arm of the coupler is recombined with the remaining Sp-Ch (from which the sixth Sb-Ch has been removed) by means of a third 2:1 coupler. De-correlating fibers are inserted for temporally shifting the Sp-Ch and the sixth Sb-Ch during recombination to emulate crosstalk over the sixth Sb-Ch and its neighbors. The node terminates with a second flexgrid LCoS-WSS, which reinserts the reconstituted Sp-Ch into the WDM multiplex. The signal spectra at the various "key" locations inside the FOX-C node are represented in Fig. 6. The spectrum labeled 4 shows that the extinction ratio of the OPBF (~25 dB) does not permit the total rejection of the neighboring sub-bands.

We first fix the optical signal-to-noise ratio (OSNR) in 0.1 nm to a value of 22.5 dB, which ensures a bit-error ratio (BER) of 10^{-4} for the MB-OFDM signal (BW = 18 GHz, GB = 2 GHz) in BtB when the FOX-C node is not in the experiment. We then introduce the node between the transmitter and receiver. We set the OPBF bandwidth to 19 GHz and vary the OSBF bandwidth from 21 up to 26 GHz, while measuring the BER of Sb-Chs 5, 6, and 7. Figure 7 presents the optimization results. The orange curve represents the BER of the central sub-band (sub-band 6). The BER of the neighboring left/right-hand Sb-Chs (Sb-Chs 5 and 7) is shown by the red curve. The crosstalk over the central Sb-Ch between the added and residual signal is maximum and minimum at low and high bandwidths, respectively, of the OSBF. The opposite observation can be made for the "pass-through" sub-bands 5 and 7 for which a large OSBF results in high spectral distortions.

The optimum OSBF bandwidth results from a trade-off between the distortions affecting the central Sb-Ch on the one hand, and degradations impairing neighboring Sb-Chs 5 and 7 on the other hand, and is thus obtained at the intersection of the orange and red curves. This measurement procedure can be reproduced for various OPBF bandwidths from 16 to 21 GHz. The gray "parabolic" curve is then obtained and shows that the optimum bandwidths of the HSR-OSBF and HSR-OPBF have values of 23 GHz and 19 GHz, respectively. The corresponding BER is equal to $\sim 2.5 \times 10^{-3}$ for the three sub-bands under concern, which is below the FEC threshold (fixed here to a BER of 2×10^{-2} corresponding to a commonly used soft-decision FEC with 20% overhead [25,26]).

In order to improve the performance of the add/drop process with the perspective of transmission through a number of cascaded FOX-C nodes, we examine in Fig. 8 the BER of each sub-carrier constituting the OFDM signal for the three Sb-Chs under study (Sb-Chs 5, 6, and 7). A degradation of the BER performance is observed for the sub-carriers that are located at the two edges of the central Sb-Ch (Sb-Ch 6), at the right-hand edge of the left-hand Sb-Ch (Sb-Ch 5) and at the left-hand edge of the right-hand Sb-Ch (Sb-Ch 7). This degradation is due to the distortions experienced by these border sub-carriers while going through the OADM and in particular to the higher attenuation experienced on the sub-band edges. To improve the performance of the add/drop multiplexing process, the idea is to eliminate the most impaired sub-carriers from the BER calculation, of course, at the expense of a spectral efficiency reduction. The sub-carrier elimination is performed at the receiver side. BER calculation bandwidths of 15 and 16.5 GHz occur when, out of 576 sub-carriers, 96 and 48 sub-carriers, respectively, are removed from the BER estimation. The net bit rate per Sb-Ch is then reduced from 100 Gbps to 83.3 Gbps and 91.6 Gbps, respectively.

Figures 9 and 10 present the OSNR sensitivity curves (BER versus OSNR) of OFDM sub-bands 5, 6, and 7 in BtB with and without the FOX-C node for three Sb-Ch

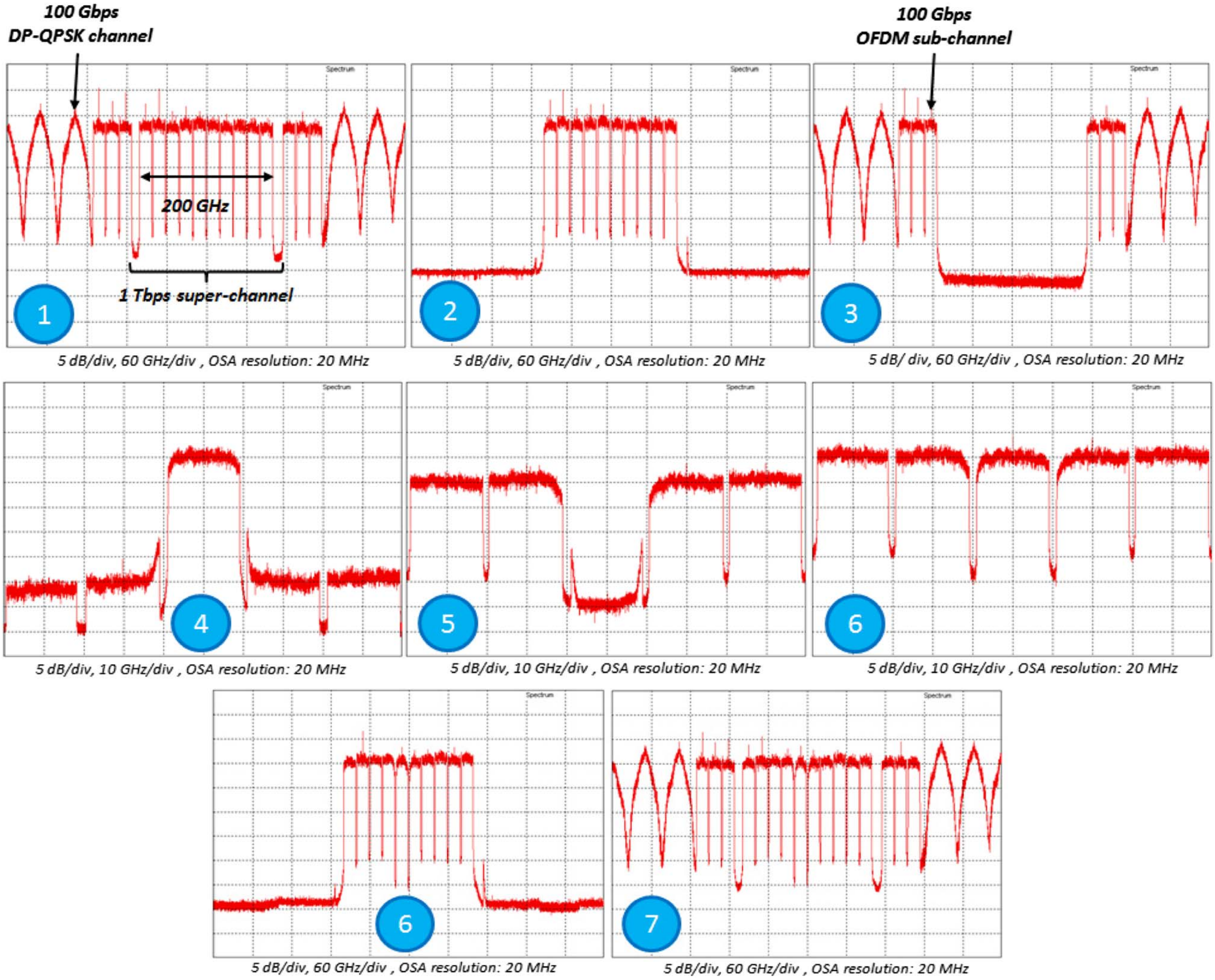

Fig. 6. Signal spectra at the various "key" locations (labeled by numbers from 1 to 7) inside the FOX-C node in the case of the MB-OFDM Sp-Ch. Two spectra are shown for the location labeled 6: the overall Sp-Ch and a zoom of its central part (where the optical add/drop multiplexing operation is performed).

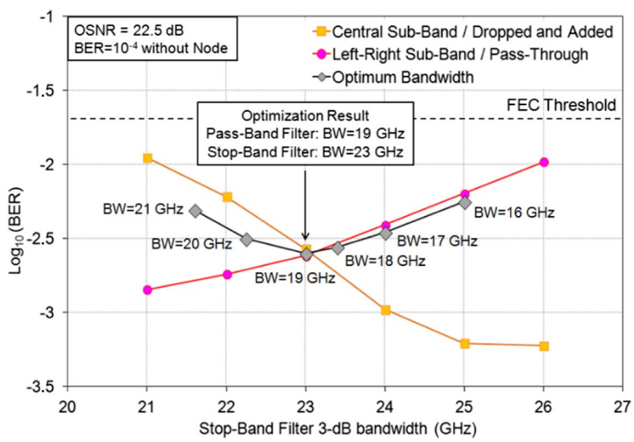

Fig. 7. BER versus the bandwidth (BW) of the OSBF for the central Sb-Ch 6 and the neighboring left/right-hand Sb-Chs (Sb-Chs 5 and 7) for various BWs of the OPBF in the case of the MB-OFDM Sp-Ch (BW = 18 GHz, GB = 2 GHz).

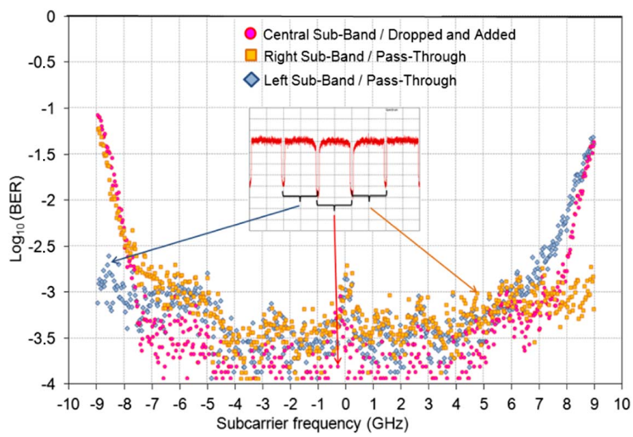

Fig. 8. BER of the various sub-carriers making up Sb-Chs 5, 6, and 7 after being routed through the OADM for the optimum bandwidth of the OPBF (BW = 19 GHz) and OSBF (BW = 23 GHz) in the case of the MB-OFDM Sp-Ch (BW = 18 GHz, GB = 2 GHz).

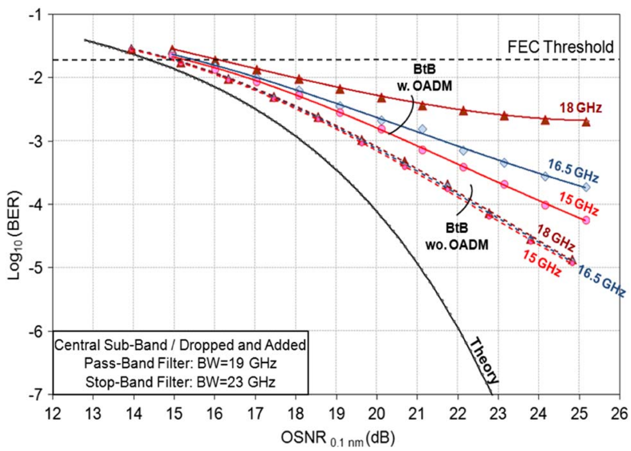

Fig. 9. BER versus OSNR (in 0.1 nm) of the central Sb-Ch (Sb-Ch 6) in BtB with (w.) and without (wo.) the FOX-C node. Measurements are performed for several BER calculation BWs (i.e., 18, 16.5, and 15 GHz). The OPBF and OSBF are tuned at the previously determined optimum BW values.

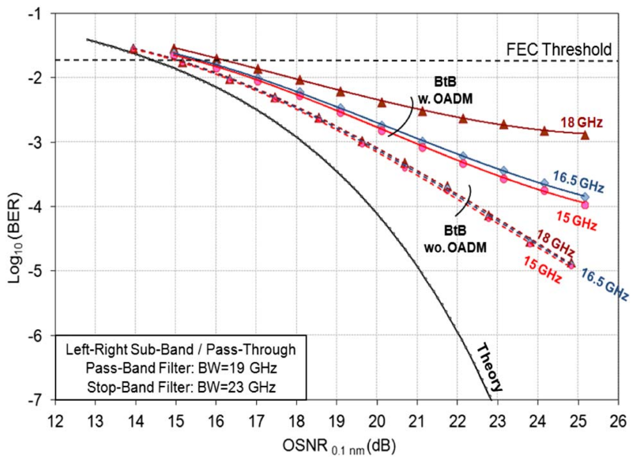

Fig. 10. BER versus OSNR (in 0.1 nm) of the left/right-hand Sb-Chs (Sb-Chs 5 and 7) in BtB with (w.) and without (wo.) the FOX-C node. Measurements are performed for several BER calculation BWs (i.e., 18, 16.5, and 15 GHz). The OPBF and OSBF are tuned at the previously determined optimum BW values.

bandwidths for BER calculation (18, 16.5, and 15) obtained by switching off a number of sub-carriers at the receiver. The theoretical OSNR sensitivity curve is also plotted as a reference. It can be observed that modifying the BER calculation bandwidth (at a constant OFDM Sb-Ch bandwidth of 18 GHz at the transmitter) does not modify the OSNR sensitivity of the OFDM signal in BtB without the FOX-C node. The situation drastically changes when the FOX-C node is introduced in the experiment. Decreasing the bandwidth removes the error floor present over the OSNR sensitivity curve of the 18 GHz OFDM signal and limits the OSNR penalty related to the add/drop operation to ~1 dB at a BER of 1×10^{-3} for the 15 GHz OFDM signal, irrespective of the sub-band considered.

OSNR sensitivity curves plotted for various BER calculation bandwidths allow us to infer the OSNR penalty of the OFDM signal as a function of its spectral support. Figure 11 presents an OSNR penalty at a BER of 1×10^{-3} for various spectral bandwidths (or equivalently spectral efficiencies) for Sb-Chs 5, 6, and 7. The OSNR penalty reaches a floor (~1 dB) when the spectral efficiencies are lower than 4.16 bit/s/Hz or equivalently when bandwidths are below 15 GHz. The higher floor penalties observed over Sb-Chs 5 and 7 are due to an insufficient rejection of the OPBF (as observed in the spectra shown in Fig. 6).

It is thus now interesting to compare the above results with the performance of the FOX-C node in BtB when the 1 Tbps MB-OFDM Sp-Ch is replaced by its N-WDM counterpart, whose Sb-Chs have a bandwidth of 15 GHz and are separated by 5 GHz guard-bands. OSNR sensitivity curves of N-WDM are plotted in Fig. 12 and compared with those of MB-OFDM (in the particular case of a bandwidth of 15 GHz). First, one can note that the central Sb-Ch shows a better performance than the left/right-hand Sb-Chs. Indeed, the central Sb-Ch suffers from distortions on both sides of its spectrum, while the left/right-hand Sb-Chs experience a single-side but more severe distortion (as shown in spectra 4 and 5 of Fig. 6). Furthermore, as explained at the end of the previous paragraph, the insufficient rejection of the OPBF (with respect to the OSBF) generates a higher crosstalk over the edge Sb-Chs 5 and 7. Second, Fig. 12 shows a slightly better performance of N-WDM compared to MB-OFDM in the presence of the OADM, coming essentially from an improved performance of the N-WDM format in BtB (i.e., without the OADM). However, better performance homogeneity is obtained after the add/drop multiplexing process between the central and left/right-hand Sb-Chs for MB-OFDM than for N-WDM. A ~1 dB OSNR penalty is measured at a BER of 1×10^{-3} for the left/right-hand N-WDM Sb-Chs with respect to the central one. The observed phenomenon is probably due to a higher sensitivity of the N-WDM format to

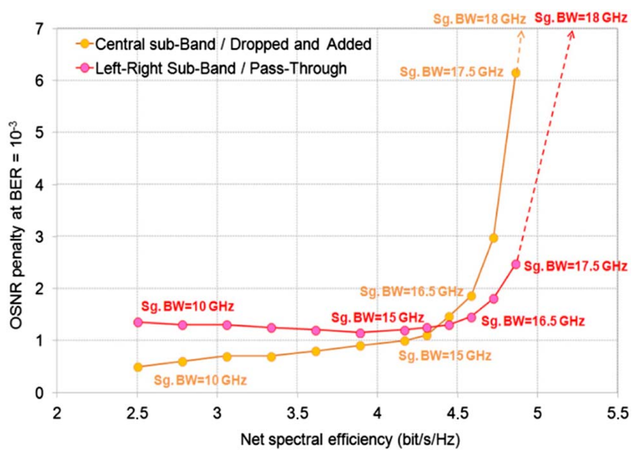

Fig. 11. OSNR penalty for a BER of 1×10^{-3} as a function of the net spectral efficiency for the central Sb-Ch (Sb-Ch 6) and left/right-hand Sb-Chs (Sb-Chs 5 and 7) after going through the FOX-C node.

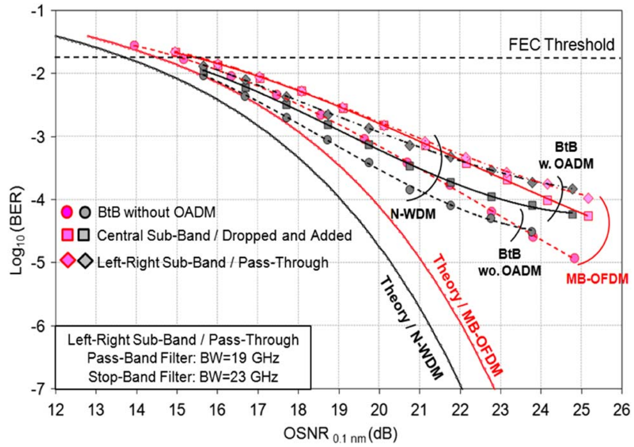

Fig. 12. BER versus OSNR (in 0.1 nm) in BtB for the N-WDM (black) and MB-OFDM (red) Sp-Chs with or without the FOX-C node. The MB-OFDM Sp-Ch is in its 15 GHz BW configuration. The OPBF and OSBF are tuned at the determined optimum BW values.

distortions of its spectrum with respect to the MB-OFDM scheme. Finally, note that an error floor appears on the OSNR sensitivity curve of N-WDM in BtB (without the OADM presence), which is probably an indication of hardware imperfections (due to Tx/Rx bandwidth distortions and DAC/ADC limited resolution [27]) and DSP limitations for 15 Gbaud 16QAM N-WDM format.

C. FOX-C Node Performance in Transmission

As described in Fig. 4, the FOX-C node is now inserted in the $N \times 100$ km G.652 fiber line for transmission evaluation. Transmission without the FOX-C node is first performed to determine the optimum power per Sb-Ch to be launched into the G.652 fiber spans. In a second step, the FOX-C node is inserted in the middle of the optical link and the performance degradation is successively measured at a distance of 400, 600, 800, and 1000 km for both MB-OFDM and N-WDM Sp-Chs.

As shown in Fig. 4, the transmission line is composed of a maximum of 10 spans of G.652 fiber (loss: 0.2 dB/km and dispersion: 17 ps/nm/km at 1550 nm), separated by EDFA with 20 dB gain and 4.5 dB noise figure (NF). In the middle of the optical link, a dynamic gain equalizer (DGE) is inserted in order to flatten the multiplex power at the receiver side after 400, 600, 800, or 1000 km, but also to achieve as much as possible equivalent OSNR for the various channels at the receiver side. A DGE in the middle of the link can lift a "low power" channel and reduce a "high power" channel so that the first channel gets better OSNR during the second half of the transmission while the second channel experiences a worse OSNR. This uncompensated transmission configuration is realistic of the coherent 100 Gbps WDM systems currently deployed over operators' OTNs, offering significantly enhanced performance compared to legacy dispersion-managed systems. When the FOX-C node is inserted, it is introduced just after the DGE.

The curves plotted in Fig. 13 present the BER as a function of the span input power per Sb-Ch in the case of the MB-OFDM Sp-Ch, when the 15 GHz bandwidth configuration is chosen and no OADM is inserted into the link. These curves allow us to determine the optimum Sb-Ch power to be injected into the fiber spans from 400 to 1000 km transmission reach. The BER of the central Sb-Ch (Sb-Ch 6) and its left/right-hand neighbors (Sb-Chs 5 and 7) (gray and purple symbols, respectively) after transmission through N/2 fiber spans, one OADM, and N/2 fiber spans are then measured and plotted in Fig. 13. It can be seen that the introduction of the FOX-C node does not degrade the transmission performance very much (less than two-tenths of a decade). The filtering impairments and spectral crosstalk inside the HSR-OADM are thus well-controlled. The BER of the central and left/right-hand Sb-Chs are below the FEC threshold, irrespective of the distance under study, which guarantees error-free transmission up to 1000 km. Good performance homogeneity also exists between the central and left/right-hand Sb-Chs.

Figure 14 is equivalent to Fig. 13 but for the N-WDM Sp-Ch. When the OADM is not inserted into the link, we observe a small BER improvement with respect to MB-OFDM (between two- and four-tenths of a decade), combined with an increase of the optimum span input power per Sb-Ch (going from 1.5 to 2 dB). This means that N-WDM is more robust to fiber nonlinearities than MB-OFDM. The BER of the central and left/right-hand Sb-Chs after going through the transmission line and OADM are also plotted at the optimum span input power per Sb-Ch. As previously reported, less homogeneity exists between the performance of the central and left/right-hand Sb-Chs with N-WDM than with MB-OFDM (in particular, at 400 and 600 km). As for the MB-OFDM Sp-Ch, from 400 up to 1000 km, the BER of the central and left/right-hand Sb-Chs of the N-WDM

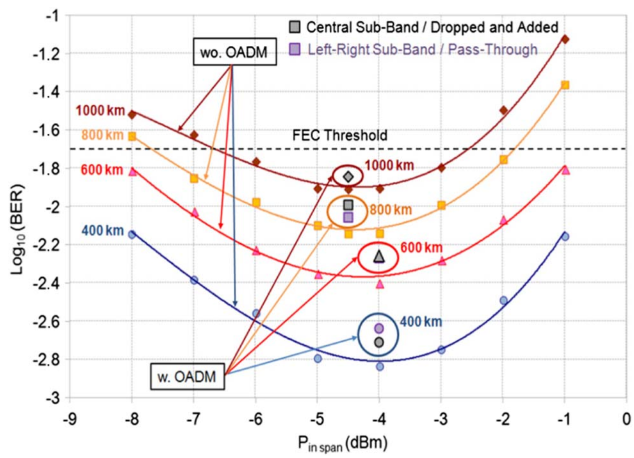

Fig. 13. BER versus span input power per Sb-Ch for the MB-OFDM Sp-Ch in the 15 GHz BER calculation BW configuration for various transmission distances (400, 600, 800, and 1000 km) when the OADM is not inserted into the link. The BER of the central and left/right-hand Sb-Chs (Sb-Chs 5, 6, and 7) after going through the OADM are also plotted over this graph (gray and purple symbols, respectively).

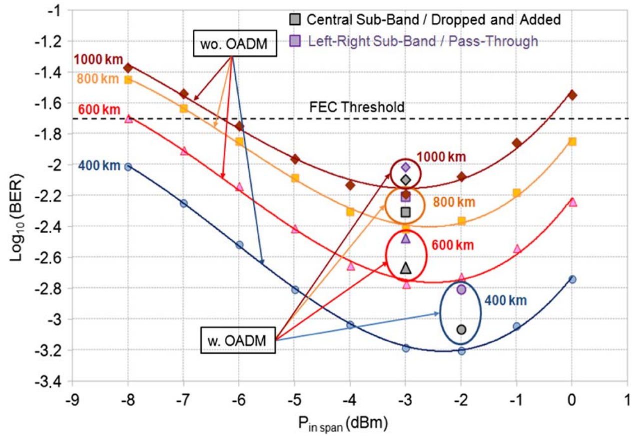

Fig. 14. BER versus span input power per Sb-Ch for the N-WDM Sp-Ch for various transmission distances (400, 600, 800, and 1000 km) when the OADM is not inserted in the link. The BER of the central and left/right-hand Sb-Chs (Sb-Chs 5, 6, and 7) after going through the OADM are also plotted over this graph (gray and purple symbols, respectively).

Sp-Ch are largely below the soft-decision FEC (SD-FEC) threshold after going through the OADM.

In these experiments, it is crucial to precisely control the drift of the laser wavelengths. The wavelength stability of the ECL sources (used both for the transmitter and LO) is typically ±3 pm (±375 MHz) per hour. It represents ±20% of the 2 GHz guard-band inserted between the Sb-Chs. Thanks to a fine spectral monitoring of the Sp-Ch (through a 20 MHz high-resolution optical spectrum analyzer), the eventual wavelength drifts are compensated manually. Observation of the symmetry of the error vector magnitude (EVM) versus sub-carriers' curve is also very useful. It allows us to control the Sb-Ch under measurement so that it is well-centered on the OPBF and OSBF transfer function. Of course, in a real network environment, accurate wavelength lockers should be implemented to ensure that laser drifts are minimal.

To put into perspective these experiments with respect to previous studies on spectral sub-wavelength switching [12,14,28,29], it can be noted that our demonstration combines the following high-performance features: high-speed Sp-Ch (1 Tbps) with high data-rate Sb-Chs (100 Gbps), higher-order QAM constellation (16QAM), reduced guard-band (2 to 5 GHz), OADM able to add/drop only one Sb-Ch, very steep high-spectral resolution (1 GHz) optical pass-band and stop-band filters with ultra-fine spectral granularity (400 MHz), and finally enhanced transmission reach (1000 km). With respect to the sensitivity of MB-OFDM and N-WDM formats to fiber nonlinear effects, the results obtained here confirm those obtained before in [30,31].

Note at last that further experiments are under progress to evaluate the tolerance of MB-OFDM and N-WDM formats to a cascade of HSR-OADM. This study is performed through the insertion of the FOX-C node into a recirculating loop. These results will be presented in upcoming papers.

V. Electronic Versus Optical Aggregation in Multi-Layer Transport Networks

The feasibility of an ultra-selective Sb-Ch optical switch has been extensively demonstrated above. To quantify the potential benefits of the proposed solution, we carry out hereafter a thorough and holistic techno-economic analysis comparing the performance of an all-optical traffic grooming (AOTG) solution, based on the route and select colorless directionless node architecture implemented in the FOX-C node, presented schematically in Fig. 15, with that of an electronic aggregation solution based on an OTN electronic switching technique. By using an in-house multi-layer optimization tool, we evaluate the spectrum and total equipment cost savings resulting from the use of the FOX-C node and AOTG.

A. Cases Under Study and Assumptions

We propose to compare four scenarios to highlight AOTG advantages. The spectrum allocation schemes for these four scenarios are illustrated in Fig. 16. Scenarios S0 and S1 are used as benchmarks.

Scenario S0 refers to the well-known coherent 100 Gbps DP-QPSK WDM systems that are currently deployed on uncompensated transmission lines equipped with G.652 fiber and EDFA (with a NF = 5 dB). SD-FEC providing further 2.5 dB OSNR margin with respect to the first generation of coherent 100 Gbps DP-QPSK WDM interfaces (based on hard-decision FEC) is implemented for a maximum transmission reach of 2000 km [12].

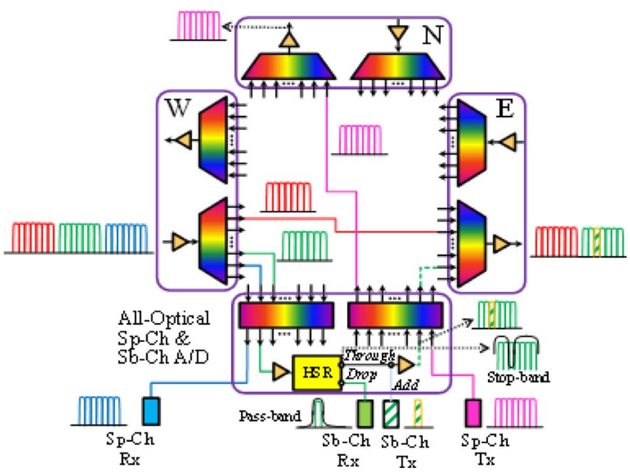

Fig. 15. FOX-C node architecture and operation. Three Sp-Chs (red, green, and blue) composed of multiple Sb-Chs enter the node from the W direction. The third Sb-Ch in the green Sp-Ch needs to be dropped and replaced with a new added Sb-Ch (green striped). The green Sp-Ch is first routed by the W ingress WSS to the Sp-Ch-level add/drop module, which directs the signal to a HSR filter with two outputs: a "drop" port (pass-band function) connected to a Sb-Ch receiver and a "through" port operating as a stop-band filter. A new Sb-Ch can now be added to the Sp-Ch output from the "through" port, which is routed to the E egress WSS.

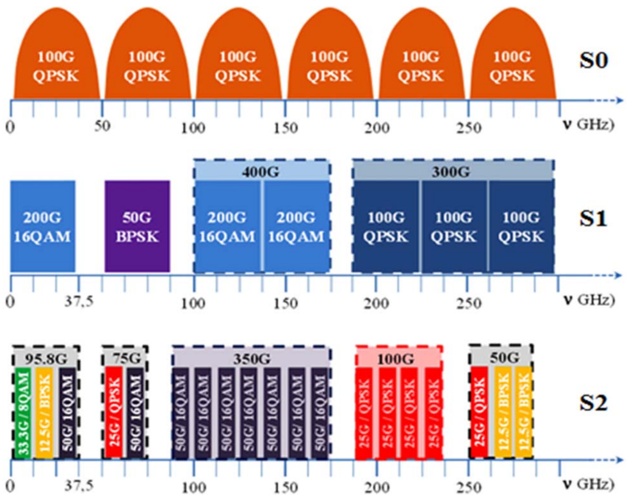

Fig. 16. Spectrum management of the WDM reference scenario (S0), the N-WDM Sp-Ch as proposed today (S1), and AOTG enabled by the MB-OFDM technique (S2).

Scenario S1, on the other hand, corresponds to a short-term and popular implementation of flexible optical networking that allows higher transport capacity thanks to improved spectral efficiency. It relies on an end-to-end N-WDM Sp-Ch transmission, where each Sb-Ch is generated by a flex rate single-carrier interface operating at 32 Gbaud (including the 20% SD-FEC overhead [25,26]). The Sb-Ch data rate is varied by selecting a modulation format adapted to the path length (50 Gbps DP-BPSK for link length up to 4000 km, 100 Gbps DP-QPSK for link length up to 2000 km, or 200 Gbps DP-16QAM for link length up to 400 km [12,14,32,33]). The Sb-Chs inside a Sp-Ch are shaped by Nyquist filters, so that each Sb-Ch is constrained to a spectral width of 37.5 GHz. A 12.5 GHz guard-band is reserved on both sides of the resulting Sp-Ch to ensure minimal filtering penalties at the reconfigurable optical add-drop multiplexers (ROADM).

To maximize the return-on-investment (RoI) from new optical network deployments and limit over-dimensioning, operators make every attempt to optimize the filling of optical channels by performing aggregation, be it in the optical or in the electronic domain. Scenario S2 refers to an AOTG solution, based on the MB-OFDM transmission scheme (as described before) and the FOX-C node enabled by the ROADM architecture shown in Fig. 15. Sp-Ch capacity can be increased or decreased by choosing the right modulation format, the number of sub-carriers forming each OFDM Sb-Ch, or the number of Sb-Chs per Sp-Ch [34]. In scenario S2, various modulation formats can be selected for Sb-Ch according to the required data rate and transmission distance, namely: DP-BPSK (12.5 Gbps, 4000 km), DP-QPSK (25 Gbps, 2000 km), DP-8QAM (33.3 Gbps, 750 km), and DP-16QAM (50 Gbps, 400 km) [12,14,32,33]. In the present study, we consider Sb-Chs with 12.5 GHz spectral width including a guard-band of 2–4 GHz between Sb-Chs in line with our previous experimental studies. Moreover, as we did in scenario S1, a 12.5 GHz guard-band is reserved between Sp-Chs [34]. Note that in S1 Sp-Chs are routed as an end-to-end entity along the network without the possibility to optically switch Sb-Chs inside the Sp-Ch, whereas in S2, the Sp-Ch entity may optically aggregate different Sb-Chs carrying various traffic demands.

Finally, scenario S0_OTN presents a case in which electronic OTN switching is used to perform traffic aggregation. In this scenario, all traffic demands, including IP demands terminated at the router and leased line (LL) demands terminated at the OTN switch, are mapped to the optical layer through this additional OTN layer inserted between the packet and transmission layers. With respect to S0, small demands can be aggregated into appropriate OTN containers before being transported over the optical channel. Therefore, from a functional point of view, S0_OTN and S2 offer similar transport and aggregation service; the main difference is that the former performs aggregation in the electronic domain, while the latter does it all optically.

Having described the scenarios under investigation, we now carry out a techno-economic analysis to estimate the approximate amount of resources, in terms of number of transceivers and ROADMs, required to accommodate a given traffic demand so that a blocking-free (B-free) connection establishment can be guaranteed while minimizing the total network cost (TNC). In this study, a spectral occupancy contribution (Avg.S) has also been included in the optimization objective (i.e., the TNC) in order to optimize simultaneously both network equipment cost and spectrum utilization. Indeed, as the saved spectrum can be used to accommodate extra services, it can be seen as a potential revenue-generation element.

We start by comparing S2 with the benchmarking scenarios S0 and S1. To accommodate traffic demands more efficiently in the network, we use an upgraded version of the impairment-aware AOTG-capable routing, modulation level and spectrum allocation algorithm described in [35] with the simulated annealing (SA) process (i.e., local extremum trap) and implement a load balancing procedure. We then carry out a multi-layer capital expenditure (CAPEX) analysis to compare the two scenarios in which aggregation is performed: the current electronic-based solution using the OTN layer (S0_OTN) and the AOTG solution (S2). To find the best multi-layer path construction and ensure that traffic demands are carried in the most effective way over the network, we use a dedicated in-house multi-layer optimization tool based on a simulated annealing meta-heuristic.

We perform our optimization studies over a national transport network typical of transmission backbones deployed in Europe by incumbent operators [12]. The network topology consists of 51 nodes connected together with 75 WDM links with a mean nodal degree of 2.9 and an average link length of 217 km. A total spectrum of 4.8 THz (C-band) using the ITU-T 12.5 GHz grid is available on all network links. The traffic matrix associated with this topology is composed of 371 demands that represent ~7 Tbps of ingress traffic in the initial year (2014). The contribution of IP traffic (terminated at the IP routers) is twice as important as that of the LL demands, representing

TABLE I
COST OF THE MULTI-LAYER TRANSPORT NODE RELATIVE TO 10G TRANSPONDER COST

Item	Cost
IP router	
Router (shelf and switch fabric)	1.62
10GE interface card	5.08
100GE interface card	8.42
OTN switch	
Shelf size 1 (0.8 Tbps, 16 slots)	10.15
Shelf size 2 (1.6 Tbps, 16 slots)	12.77
Shelf size 3 (1.6 Tbps, 32 slots)	17.47
Shelf size 4 (3.2 Tbps, 32 slots)	20.91
100 Gbps colored line interface	9.59
10 × 10GE client interface card	2.65
1 × 100GE client interface card	5.56
Flexible optical node	
Degree 1, ROADM (color/directionless)	11.45
Degree 2, ROADM (color/directionless)	16.03
Additional degree, ROADM (color/directionless)	4.58
Coarse add/drop stage	6.77
10GE client interface	0.04
100GE client interface	4.17
"Muxponder/transponder" w/o client interface	6.86
Sub-band of at least 3 slots	6.86
Sub-band of 2 slots (specific scenario S2)	5.28
Sub-band of 1 slot (specific scenario S2)	3.71
Ultra-selective add/drop element (for S2)	1–20

time-domain-multiplexing (TDM) traffic (terminated at the ROADMs or OTN switches as a function of the scenario chosen). Note that the traffic matrix used here has been extracted from a real transport network and consequently does not show a uniform distribution across the nodes since some nodes are used for pure transit, whereas others can manage up to 300 Gbps of edge services.

Table I presents the relative costs (using the cost of a 10G transponder as a reference) considered in our multi-layer node model. For the IP router and OTN switch elements, the cost model has been elaborated from an average of real equipment prices provided by vendors as indicated in [12,36]. For the flexible optical node part, cost items follow the route and select ROADM architecture detailed in [37]. In Table I, we assumed a relative cost for the ultra-selective add/drop (U-A/D) element ranging from 1 to 20 to account for the effect of technology maturity and mass production on the relative final network value. This item is subject to a specific sensitivity analysis.

B. Simulation and Optimization Results

To start the techno-economic analysis, let us leave aside the multi-layer network scenario S0_OTN for now and focus rather on the network scenarios S0, S1, and S2, assuming only one G.652 fiber per link and per direction (and thus no parallel systems). We look to answer the question of how long and at what cost it is possible to support a B-free connection in each scenario considering a 35% annual traffic growth [38], and ultra-high-resolution optical filtering technology immaturity (U-A/D cost equal to 20).

Figure 17(a) shows the Avg.S in the period from 2014 to 2023. S2 (AOTG) outperforms S0 and S1 every single year of the period under consideration, and its benefits are twofold. First, it shows a spectral occupancy improvement ranging from ~70% in the initial year (2014), representing a low-load scenario, down to ~30% in the last year in which S1 can support a B-free connection establishment (2021). This behavior can be explained by the grooming capability brought about by S2, which allows aggregating small connections into larger units (Sp-Chs), thus saving spectrum resources through the elimination of the large guard-bands between 100 Gbps channels in S0 and Sp-Chs in S1. The grooming capability of S2 therefore leads to more significant spectral occupancy improvement for low loads, as observed in Fig. 17(a). Second, S2 increases the network lifespan by two years (from 2021 to 2023), which can translate into revenue and somewhat alleviate the cost of migrating to parallel fiber systems or multi-band (i.e., C + L band) transmission systems [39]. Depending on the net annual revenue (NAR), the S2 network migration

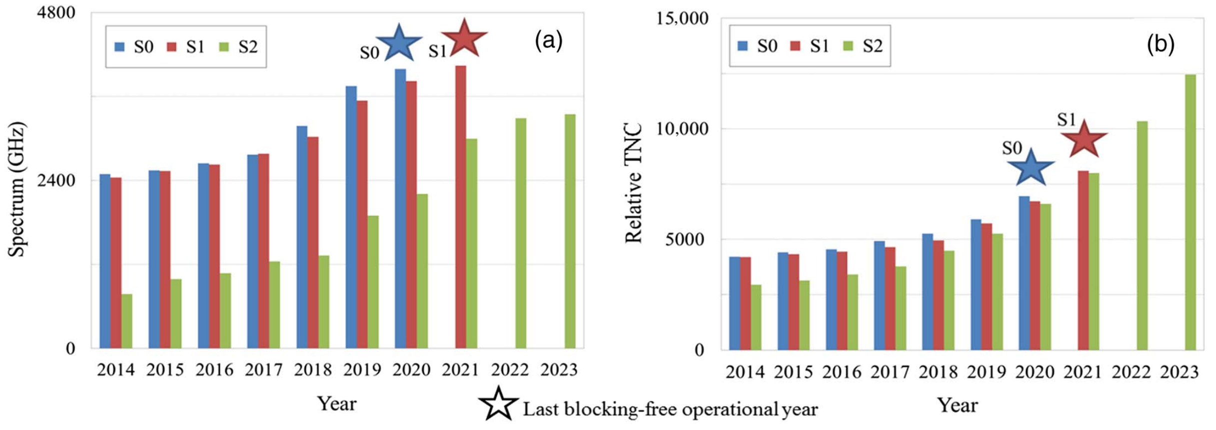

Fig. 17. (a) Avg.S in GHz and (b) relative TNC with respect to 10 Gbps transceiver cost for the period from 2014 to 2023. Last B-free operational years for S0 and S1 are 2020 and 2021, respectively.

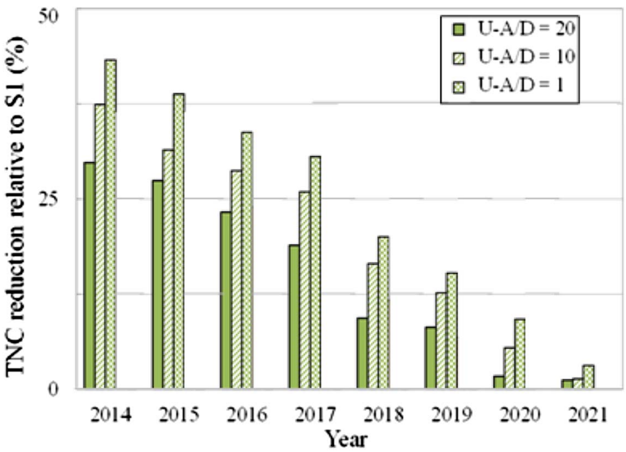

Fig. 18. TNC improvement for different cost values of the U-A/D for the S2 scenario compared to the S1 scenario over the period where the two scenarios support B-free connection establishment.

toward a multi-fiber/multi-band scenario could provide savings equal to 2 × NAR with respect to S1.

Figure 17(b) shows, in turn, the TNC for the period from 2014 to 2023. S2 produces cost savings starting at ~30% compared to S1 in 2014 and reducing gradually as the offered load to the network increases (savings amounting to ~5% are obtained in 2021). An explanation for this reduction in TNC savings is that the current analysis has not captured the impact of U-A/D technology maturity and mass production on the resulting TNC reduction.

To quantify the effect on the TNC of reducing the cost of the U-A/D stage in S2, we conducted a sensitivity analysis on this parameter. The result is shown in Fig. 18. As can be observed, any reduction in the cost of the U-A/D technology has a clear impact on the TNC, decreasing it by ~4%–8% (for U-A/D = 10) and ~7%–13% (for U-A/D = 1).

Up to now, we have demonstrated the benefits of the AOTG solutions in terms of both Avg.S and TNC with respect to the other network scenarios that do not incorporate this feature. We now turn our attention to the comparison between optical and electronic OTN-based aggregation. To do that, we consider a multi-layer network able to perform electronic aggregation at both IP routers and OTN switches by taking care that all traffic demands are mapped into the optical layer through the OTN layer (scenario S0_OTN).

We undertake the study for scenarios S2 and S0_OTN by employing an in-house multi-layer optimization tool [36], which optimizes the global multi-layer network cost. In the S0_OTN scenario, the optimization process takes into account IP, OTN, and WDM layers but only the WDM layer when scenario S2 is considered (since aggregation in S2 is performed exclusively in the FOX-C nodes).

In Fig. 19, we present the results of the comparison between the relative network cost for scenarios S2 and S0_OTN over the period from 2014 to 2023. As indicated in Fig. 19, the total relative network cost in the multi-layer scenario comprises three values: 1) the optical layer cost (cost_Opt), i.e., the cost of optical equipment in the optical layer; 2) the OTN layer cost (cost_OTN), i.e., the total cost of the OTN switches in the network; and 3) the IP cost (cost_IP), i.e., the cost related to the IP routers (cf. Table I). Conversely, in the AOTG scenario (S2), only cost_Opt has been considered. If we now compare the TNC for S2 in Fig. 17(b) with the cost_Opt for scenario S2 in Fig. 19 (each graph having been obtained using a different optimization tool), we observe that results are in good agreement. Figure 19 shows that, even though S0_OTN leads to a better cost_Opt value compared to S2, S0_OTN's total relative network cost is considerably higher than that of S2 (e.g., ~50% higher in the whole range of study). The reason behind this situation is that, in an OTN-based scenario, a better cost_Opt performance (due to the minimization of

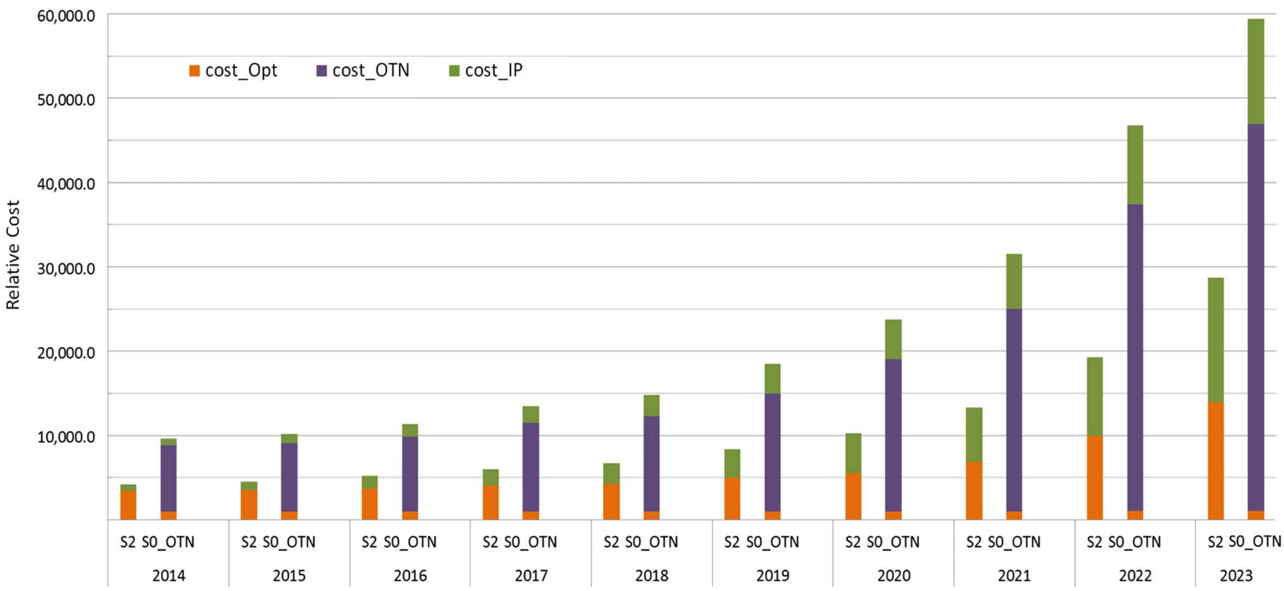

Fig. 19. Relative network cost (optical, OTN, and IP layers) of S2 versus S0_OTN over a period of 10 years (2014–2023).

the required number of transceivers) comes at the expense of higher cost_OTN, which scales up much faster than the U-A/D cost for AOTG.

VI. Conclusions and Perspectives

In this article, we give a general overview of the FOX-C project, which aimed at developing the tools (i.e., the flexible optical cross-connect element) that allow fully flexible optical networking. Full photonic elasticity supposes that optical switching acts over not only Sp-Chs but also their tributaries (i.e., Sb-Chs) with the aim of obtaining a better fulfillment of wavelengths and spectrum in optical transport networks to delay the apparition of the "capacity crunch." After having presented the concepts of our work, the key component of the FOX-C node (i.e., a high spectral resolution optical pass-band and stop-band filter) is described. It provides finer than 1 GHz optical resolution and 400 MHz spectral granularity with an extinction ratio of ~25 dB. This HSR optical filter is then used in an ultra-selective add-drop node (FOX-C), which is inserted in an experimental test-bed with MB-OFDM and N-WDM advanced modulation formats, in order to evaluate its performance both in back-to-back and in a G.652 fiber-based transmission line. The FOX-C add-drop multiplexer is applied over a 1 Tbps MB-OFDM or N-WDM Sp-Ch with 5 bit/s/Hz net spectral efficiency composed of ten 100 Gbps Sb-Chs spaced by 20 GHz. The FOX-C node successfully separates the sub-channels without generating crippling filtering impairments and crosstalk. Uncompensated transmission over 1000 km of G.652 fiber using a 16QAM modulation format is demonstrated in the presence of the FOX-C node. Finally, in the last part of the article, a techno-economic analysis is performed to show the potential of our all-optical traffic grooming approach in a typical European multi-layer long-haul transport network, and its economic superiority is compared to the electronic OTN-based aggregation solution. Our results indicate that we need more filtering device efforts to help realize FOX-C commercially, as it clearly shows advantages in supporting more traffic more economically.

Acknowledgment

This research was supported by the FP7 EU-funded project FOX-C under grant agreement no. 318415.

References

[1] M. Jinno, H. Takara, B. Kozicki, Y. Tsukishima, Y. Sone, and S. Matsuoka, "Spectrum-efficient and scalable elastic optical path network: Architecture, benefits, and enabling technologies," *IEEE Commun. Mag.*, vol. 47, no. 11, pp. 66–73, 2009.

[2] O. Gerstel, M. Jinno, A. Lord, and S. J. B. Yoo, "Elastic optical networking: A new dawn for the optical layer?" *IEEE Commun. Mag.*, vol. 50, no. 2, pp. s-12–s-20, 2012.

[3] A. D. Ellis and F. C. G. Gunning, "Spectral density enhancement using coherent WDM," *IEEE Photon. Technol. Lett.*, vol. 17, pp. 504–506, 2005.

[4] R. Ryf, Y. Su, L. Moller, S. Chandrasekhar, X. Liu, D. T. Neilson, and C. R. Giles, "Wavelength blocking filter with flexible data rates and channel spacing," *J. Lightwave Technol.*, vol. 23, no. 1, pp. 54–61, Jan. 2005.

[5] S. Poole, S. Frisken, M. Roelens, and C. Cameron, "Bandwidth-flexible ROADMs as network elements," in *Optical Fiber Communication Conf.*, Los Angeles, CA, 2011, paper OTuE1.

[6] D. Sinefeld, S. Ben-Ezra, and D. M. Marom, "Nyquist-WDM filter shaping with a high-resolution colorless photonic spectral processor," *Opt. Lett.*, vol. 38, pp. 3268–3271, 2013.

[7] R. Rudnick, A. Tolmachev, D. Sinefeld, O. Golani, S. Ben-Ezra, M. Nazarathy, and D. M. Marom, "Sub-banded/single-sub-carrier drop-demux and flexible spectral shaping with a fine resolution photonic processor," in *European Conf. on Optical Communication*, Cannes, France, 2014, post-deadline paper PD.4.1.

[8] S. Sygletos, S. J. Fabbri, E. Giacoumidis, M. Sorokina, D. Marom, M. F. C. Stephens, D. Klonidis, I. Tomkos, and A. D. Ellis, "A novel architecture for all-optical add-drop multiplexing of OFDM signals," in *European Conf. on Optical Communication*, Cannes, France, 2014, paper We.1.5.4.

[9] X. Liu, S. Chandrasekhar, X. Chen, P. J. Winzer, Y. Pan, B. Zhu, T. F. Taunay, M. Fishteyn, M. F. Yan, J. M. Fini, E. M. Monberg, and F. V. Dimarcello, "1.12-Tb/s 32-QAM-OFDM superchannel with 8.6-b/s/Hz intra-channel spectral efficiency and space-division multiplexing with 60-b/s/Hz aggregate spectral efficiency," in *European Conf. on Optical Communication*, Geneva, Switzerland, 2011, postdeadline paper Th.13.B.1.

[10] A. Klekamp, R. Dischler, and F. Buchali, "Transmission reach of optical-OFDM super-channels with 10-600 Gb/s for transparent bit-rate adaptive networks," in *European Conf. on Optical Communication*, 2011, paper Tu.3.K.2.

[11] W. Shieh, "OFDM for flexible high-speed optical networks," *J. Lightwave Technol.*, vol. 29, pp. 1560–1577, 2011.

[12] E. Pincemin, M. Song, J. Karaki, O. Zia-Chahabi, T. Guillossou, D. Grot, G. Thouenon, C. Betoule, R. Clavier, A. Poudoulec, M. Van der Keur, Y. Jaouën, R. Le Bidan, T. Le Gall, P. Gravey, M. Morvan, B. Dumas-Feris, M. L. Moulinard, and G. Froc, "Multi-band OFDM transmission at 100 Gbps with sub-band optical switching," *J. Lightwave Technol.*, vol. 32, pp. 2202–2219, June 2014.

[13] N. Goldshtein, D. Sinefeld, O. Golani, R. Rudnick, L. Pascar, R. Zektzer, and D. M. Marom, "Fine resolution photonic spectral processor using a waveguide grating router with permanent phase trimming," *J. Lightwave Technol.*, vol. 34, pp. 379–385, Jan. 2016.

[14] E. Pincemin, M. Song, J. Karaki, A. Poudoulec, N. Nicolas, M. Van der Keur, Y. Jaouën, P. Gravey, M. Morvan, and G. Froc, "Multi-band OFDM transmission with sub-band optical switching," in *European Conf. on Optical Communication*, London, UK, 2013, paper Th.2.A.1.

[15] T. M. Schmidl and D. C. Cox, "Robust frequency and timing synchronization for OFDM," *IEEE Trans. Commun.*, vol. 45, pp. 1613–1621, Dec. 1997.

[16] J. Karaki, E. Pincemin, Y. Jaouen, and R. Le Bidan, "Frequency offset estimation robustness in a polarization-multiplexed coherent OFDM system stressed by chromatic dispersion and polarization mode dispersion," in *Conf. on Lasers and Electro-Optics*, San Jose, CA, 2012, paper CF1F.3.

[17] S. Jansen, I. Morita, T. C. W. Schenk, and H. Tanaka, "Long-haul transmission of 16 × 52.5 Gbits/s polarization-division multiplexed OFDM enabled by MIMO processing," *J. Opt. Netw.*, vol. 7, no. 2, pp. 173–182, 2008.

[18] D. Petrovic, W. Rave, and G. Fettweis, "Effects of phase noise on OFDM systems with and without PLL: Characterization and compensation," *IEEE Trans. Commun.*, vol. 55, pp. 1607–1616, Aug. 2007.

[19] A. Josten, B. Baeuerle, E. Dornbierer, J. Boesser, F. Abrecht, and D. Hillerkuss, "Multiplier-free real-time timing recovery algorithm in the frequency domain based on modified Godard," in *Advanced Photonics Congr.*, 2015, paper SpS4D.2.

[20] D. Godard, "Self-recovering equalization and carrier tracking in two-dimensional data communication systems," *IEEE Trans. Commun.*, vol. 28, pp. 1867–1875, Nov. 1980.

[21] P. J. Winzer and A. H. Gnauck, "112-Gb/s polarization-multiplexed 16-QAM on a 25-GHz WDM grid," in *European Conf. on Optical Communication*, Brussels, Belgium, 2008, paper Th.3.E.5.

[22] M. Selmi, Y. Jaouen, and P. Ciblat, "Accurate digital frequency offset estimator for coherent PolMux QAM transmission systems," in *European Conf. on Optical Communication*, Brussels, Belgium, 2009, paper P3.08.

[23] T. Pfau, S. Hoffmann, and R. Noe, "Hardware-efficient coherent digital receiver concept with feedforward carrier recovery for M-QAM constellations," *J. Lightwave Technol.*, vol. 27, pp. 989–999, Apr. 2009.

[24] X. Zhou, "Hardware efficient carrier recovery algorithms for single-carrier QAM systems," in *Advanced Photonics Congr.*, 2012, paper SpTu3A.1.

[25] K. Onohara, T. Sugihara, Y. Konishi, Y. Miyata, T. Inoue, S. Kametani, K. Sugihara, K. Kubo, H. Yoshida, and T. Mizuochi, "Soft-decision-based forward error correction for 100 Gb/s transport systems," *IEEE J. Sel. Top. Quantum Electron.*, vol. 16, pp. 1258–1267, Sept./Oct. 2010.

[26] L. E. Nelson, G. Zhang, M. Birk, C. Skolnick, R. Isaac, Y. Pan, C. Rasmussen, G. Pendock, and B. Mikkelsen, "A robust real-time 100G transceiver with soft-decision forward error correction," *J. Opt. Commun. Netw.*, vol. 4, no. 11, pp. B131–B141, Nov. 2012.

[27] X. Chen, S. Chandrasehkar, D. Randel, W. Gu, and P. Winzer, "Experimental quantification of implementation penalties from limited ADC resolution for Nyquist shaped higher-order QAM," in *Optical Fiber Communication Conf.*, Anaheim, CA, 2016, paper W4A.3.

[28] Y. Chen, J. Li, C. Zhao, Y. Zhong, Y. He, and Z. Chen, "Experimental demonstration of subband switching functionality on optical OFDM super-channel," in *European Conf. on Optical Communication*, Los Angeles, CA, 2012, paper JW2A.1.

[29] R. Dischler, F. Buchali, and A. Klekamp, "Demonstration of bit rate variable ROADM functionality on an optical OFDM superchannel," in *European Conf. on Optical Communication*, San Diego, CA, 2010, paper OTuM7.

[30] Y. Lu, Y. Fang, B. Wu, K. Wang, W. Wan, F. Yu, L. Li, X. Shi, and Q. Xiong, "Experimental comparison of 32-Gbaud electrical-OFDM and Nyquist-WDM transmission with 64GSa/s DAC," in *European Conf. on Optical Communication*, London, UK, 2013, paper We.1.C.3.

[31] J. Karaki, E. Giacoumidis, D. Grot, T. Guillossou, C. Gosset, R. Le Bidan, T. Le Gall, Y. Jaouën, and E. Pincemin, "Dual-polarization multi-band OFDM versus single-carrier DP-QPSK for 100 Gb/s long-haul WDM transmission over legacy infrastructure," *Opt. Express*, vol. 21, pp. 16982–16991, July 2013.

[32] O. Z. Chahabi, D. Grot, T. Guillossou, and E. Pincemin, "Coherent optical transmission at 40 Gbps and 100 Gbps over 1000 km of DCF-free G.652 and G.655 fibre infrastructure," in *Optical Fiber Communication Conf.*, San Francisco, CA, 2014, paper W2A.14.

[33] Y. Loussouarn, E. Pincemin, M. Song, S. Gauthier, Y. Chen, and S. Zhong, "400 Gbps coherent real-time Nyquist-WDM DP-16QAM transmission over legacy G.652 and G.655 fibre infrastructure with 2-dB margin," in *Optical Fiber Communication Conf.*, Los Angeles, CA, 2015, paper W3E.3.

[34] G. Thouenon, C. Betoule, P. S. Khodashenas, J. M. Rivas-Moscoso, D. Klonidis, E. Le Rouzic, and E. Pincemin, "Electrical v/s optical aggregation in multi-layer optical transport networks," in *IEEE Conf. on Photonics in Switching*, Florence, Italy, 2015, paper WeIII1-2.

[35] P. S. Khodashenas, J. M. Rivas-Moscoso, D. Klonidis, G. Thouenon, C. Betoule, and I. Tomkos, "Impairment-aware resource allocation over flexi-grid network with all-optical add/drop capability," in *European Conf. on Optical Communication*, Valencia, Spain, 2015, paper P.6.13.

[36] G. Thouenon, C. Betoule, E. Pincemin, P. S. Khodashenas, J. M. Rivas-Moscoso, and I. Tomkos, "All-optical vs. electrical aggregations CAPEX comparisons in a fully-flexible multi-layer transport network," in *European Conf. on Optical Communication*, Valencia, Spain, 2015, paper We.4.5.4.

[37] J. M. Rivas-Moscoso, S. Ben-Ezra, P. S. Khodashenas, D. M. Marom, D. Klonidis, P. Zakynthinos, and I. Tomkos, "Cost and power consumption model for flexible super-channel transmission with all-optical sub-channel add/drop capability," in *IEEE Int. Conf. on Transparent Optical Networks*, 2015, invited paper Th.B2.5.

[38] P. S. Khodashenas, J. M. Rivas-Moscoso, D. Klonidis, G. Thouenon, C. Betoule, E. Pincemin, and I. Tomkos, "Techno-economic analysis of flexi-grid networks with all-optical add/drop capability," in *Int. Conf. on Photonics in Switching*, Florence, Italy, 2015, paper ThIII2-2.

[39] B. Shariati, P. S. Khodashenas, J. M. Rivas-Moscoso, S. Ben-Ezra, D. Klonidis, F. Jiménez, L. Velasco, and I. Tomkos, "Investigation of mid-term network migration scenarios comparing multi-band and multi-fiber deployments," in *Optical Fiber Communication Conf. and Exhibition*, Los Angeles, CA, 2016, paper Th1E.1.